PAPER

Check for updates

3D-printed devices for multiplexed semi-quantitative competitive lateral flow immunoassays†

Guodong Tong,[a] Kazushi Misawa,[a] Purim Jarujamrus, [abc] Yuki Hiruta [a] and Daniel Citterio [*a]

Lateral flow immunoassays (LFIAs) are widely used for the simple and rapid detection of various targets at the point of need. However, LFIAs enabling the simultaneous detection of multiple analytes and the possibility for naked-eye semi-quantitative analysis are facing various challenges, including the requirement of large sample volumes, low efficiency, and accuracy. This is particularly the case for the competitive immunoassay format targeting the detection of low molecular weight compounds, such as, for example, drugs. Due to limited space for multiple reaction zones on a single planar nitrocellulose membrane, conducting multiplexed tests requires the addition of more test strips, which consequently increases the size of the whole device. To overcome these spatial constraints, two 3D-printed devices fitting eight assay lanes of both backed and unbacked nitrocellulose membranes have been designed. For proof of concept, 8-OHdG, caffeine, and acetaminophen were used as model analytes. Inkjet printing was applied to deposit capture reagents in the form of text symbols while controlling the concentration thresholds for text readability to achieve an intuitive result expression. A comparably small sample volume of 350 μL was sufficient to simultaneously visually distinguish 4 concentration levels of caffeine (0, 4, 10, 175 ng mL^{-1}) and acetaminophen (0, 4, 8, 12 ng mL^{-1}) in mixed solutions without crosstalk. This study demonstrates the potential of 3D-printed LFIA devices for multiplex and semi-quantitative analyte detection.

Introduction

Lateral flow immunoassays (LFIA) are paper-based analytical devices relying on antigen–antibody interactions. They are widely used in clinical diagnostics,[1] agriculture,[2] food safety control,[3] or forensic sciences[4] due to their rapidity and simple single-step assay operation. Typically, all the required reagents are pre-immobilized in advance on a nitrocellulose membrane, and other fibrous paper-like materials that are part of the devices. In most cases, colorimetric labels such as gold nanoparticles (AuNPs) or colored latex beads are used to create a signal, allowing untrained users to observe a naked-eye readable result within 5–20 minutes of the sample

aDepartment of Applied Chemistry, Keio University, 3-14-1 Hiyoshi, Kohoku-ku, Yokohama 223-8522, Japan. E-mail: citterio@applc.keio.ac.jp; Tel: +81 45 566 1568

bDepartment of Chemistry and Center of Excellence for Innovation in Chemistry, Faculty of Science, Ubon Ratchathani University, Ubon Ratchathani 34190, Thailand

cNanomaterials Science, Sensors & Catalysis for Problem-Based Projects, Faculty of Science, Ubon Ratchathani University, Ubon Ratchathani 34190, Thailand

† Electronic supplementary information (ESI) available: Details of device designs and layouts of all pads; design sketches of 3D models; composition of artificial urine; cap design of cap for devices type B and P; definition of Δgray value; relationship between combined ratio and initial concentration of Ab and Ag. See DOI: https://doi.org/10.1039/d4ay02009j

application. Compared to most instrument-based analytical methods, LFIAs have the potential to realize out of laboratory onsite analysis.

With increasing demands for medical diagnostics or drug of abuse screening in the field, it becomes increasingly important to detect multiple substances simultaneously from a single sample, which is beneficial in terms of cost reduction and improved efficiency.

The most straightforward strategy is to increase the number of test lines on a conventional LFIA strip, which requires nearly no alterations from the standard design. However, due to its small observable detection area, the commercialized LFIA design only allows the simultaneous detection of a limited number of analytes. Some specific analytes, such as identifying different strains of tuberculosis infections or antibiotics with similar core structures, can be detected by optimizing the production process of antibodies appropriate for binding with multiplex binding sites.[5-7] Although a single test enables the detection of multiple analytes for these cases, the complicated processes for antibody production and the limited analytical target range to one specific class of compound pose difficulties for widespread application.

Typical examples of LFIAs targeting multiple analytes are, for example, able to simultaneously detect two or three venom

proteins,[8] antibiotics,[9,10] allergens,[11] pesticides,[12] bacteria,[13] viruses[14] or toxins.[15,16] In addition, some examples of devices, enabling the simultaneous detection of 4–8 analytes have been reported.[17–21] However, in all these cases, the well-known general plastic cassette-type device housing concept has been sacrificed, so that the bare nitrocellulose strip's robustness would need to be improved for commercial use. In addition, a sample flowing to multiple test lines located at different downstream positions of the nitrocellulose membrane proceeds with decreasing flow speed over time, which may cause variations in the binding rate of antigens and antibodies, finally affecting the assay accuracy. A strategy alternative to multiple test lines is to replace the line display with dots in the form of a microarray spotted with numerous reactants.[22,23] However, this results in a partial sacrifice of assay robustness, since the signal of the smaller detection sites is more easily affected by inhomogeneous sample liquid flow. Another alternative method for achieving simultaneous multi-analyte detection with LFIAs is to arrange multiple individual assay strips into a single device.[24–26] This approach increases the available reaction area, allowing various test lines for multiplex testing while avoiding reciprocal interference. However, the requirement of a significantly larger sample volume can be a drawback.

Although for many cases of currently used LFIAs, a "yes or no" signaling strategy indicating either the absence or presence of an analyte is sufficient, other circumstances require a more quantitative approach. In forensic applications, for example, the intake of different amounts of hard drugs can result in varying levels of legal liability. In the case of a toxicologic emergency, the appropriate treatment will need to be adapted for different degrees of poisoning. Quantitative interpretation of LFIAs based on labels like quantum dots, magnetic nanoparticles, and enzymes requires the readout of fluorescence intensity, tunnelling magnetoresistance, or an electrochemical signal with a specific reader.[27–29] Also, for the standard colorimetric signal typified by AuNPs, quantitative signaling requires using particular imaging tools[30,31] in contrast to the naked eye interpretable qualitative assays. Hence, the development of naked-eye semiquantitative readout systems is highly important for user-friendly point-of-care testing.

One previously reported strategy for semiquantitative signal interpretation is to prepare multiple test lines targeting the same analyte with optimized capture and signaling reagent concentrations, realizing the appearance or disappearance of lines at different threshold analyte concentrations.[32] Typically, the results are determined by counting the number of visible lines and the threshold ranges can be refined to 3–4 concentration levels.[33–36] However, arranging multiple test lines for a single target to occupy the limited reaction area of a nitrocellulose strip prevents the detection of various analytes. In addition, counting the number of test lines is often not intuitive, particularly in the case of competitive immunoassays characterized by an increasing number of disappearing lines with increasing target analyte concentration.

Recently, 3D printing technology has become widely used to develop bioanalytical devices for point-of-care testing. Whether microfluidic devices or scaffolds, 3D printing provides an excellent opportunity to flexibly create complex structures.[37] In the field of LFIAs, 3D printing technologies have been employed to fabricate various sorts of accessories, which, for example, meet the demands for electrochemical analysis, quantitative detection, or user-friendly smartphone-based readout.[38–44]

In this study, a 3D-printed device has been developed, which can compactly embed 8 LFIA lanes to detect maximal 8 different analytes, or semi-quantitatively detect multistage concentration levels, using multiple lanes per analyte. Compared to existing concepts, a lower sample volume will be required. In addition, the text-based naked eye result display previously introduced by our group has been adopted instead of the line counting approach, which allows a more intuitive readout by the naked eye.[45] For proof-of-concept, three low-molecular-weight model analytes related to human health have been selected. 8-Hydroxy-2′-deoxyguanosine (8-OHdG) represents an oxidative stress biomarker, while caffeine and acetaminophen represent drugs, which may lead to addiction. The features of the developed devices have been evaluated through competitive immunoassays targeting these compounds.

Experimental section

Materials and instruments

Gold nanoparticles (AuNPs, 20 nm diameter, optical density (OD) = 1, reactant free) and 8-OHdG were purchased from Sigma-Aldrich (St. Louis, MO, USA). Bovine serum albumin (BSA), polyvinylpyrrolidone K25 (PVP K25), and polyethylene glycol 20 000 (PEG 20 000) were purchased from FUJIFILM Wako Pure Chemical Cooperation (Osaka, Japan). The 8-OHdG-BSA conjugate and the anti-8-OHdG monoclonal antibody (mAb) produced in rats were received from TechnoMedica Co., Ltd (Kanagawa, Japan). Caffeine and acetaminophen were purchased from Nacalai Tesque, Inc. (Kyoto, Japan). The following nitrocellulose (NC) membranes were used: Unisart® CN 140 Backed NC (1UN14ER100025NT) from Sartorius (Goettingen, Germany) and IAB-135 from Advantec (Tokyo, Japan). Anti-caffeine mAb and caffeine-BSA conjugate were purchased from MyBioSource, Inc. (San Diego, CA, USA). In contrast, anti-acetaminophen mAb and acetaminophen-BSA conjugate were acquired from Medix Biochemica (Espoo, Finland). All solutions were prepared using ultrapure water (18.2 MΩ cm) produced by a PURELAB flex water purification system (ELGA, Veolia Water, Marlow, UK). Cellulose fiber (CFSP203000) and glass fiber (GFDX203000) were purchased from Millipore (Billerica, MA, USA). Low VOC double-sided adhesive tape (4511-50) was purchased from 3 M (St. Paul, MN, USA). A Biospec-nano Life Science Spectrophotometer (SHIMADZU, Kyoto, Japan) was used to determine the OD when preparing the AuNP-labeled antibody conjugates Au-8-OHdG mAb, Au-caffeine mAb, and Au-acetaminophen mAb. A thermally actuated Canon PIXUS TS203 inkjet printer (Canon, Tokyo, Japan) deposited the antigen-BSA conjugates onto nitrocellulose membranes. A CanoScan 9000F Mark II scanner (Canon, Tokyo, Japan) was used to acquire color images of the nitrocellulose membranes. Quantitative colorimetric data analysis was performed using the Image J software (NIH, Bethesda, MD, USA). A Silhouette CAMEO3 electronic cutting tool from Silhouette Inc.

(Lindon, USA) was applied to cut nitrocellulose membranes, cellulose, and glass fiber pads. An Objet30 Prime 3D printer with VeroClear resin from Stratasys (Eden Prairie, MN, USA) was used to fabricate 3D-printed parts.

Design of 3D-printed device components

The CAD files for the 3D printing of device components were created with Shapr3D (Budapest, Hungary). Device type P (Fig. 1) was designed to accommodate plain non-backed NC membranes, while device type B (Fig. S1†) was designed for NC membranes with a transparent backing, commonly used for conventional LFIA devices. The complete device consists of a lid, a container, and a cap, able to hold a cellulose sample pad, adhesive tape, 8 sets of glass fiber conjugate pads and NC membranes, and an absorbent pad, all placed at fixed positions. In addition, transfer pads (TP) are used in device type B to support flow path completion.

Labelling of mAbs with AuNPs

The antibody-AuNPs conjugates were prepared through non-directional and noncovalent immobilization by physical adsorption[46] following the steps of a previously reported approach.[45] AuNP solution (1 mL in PBS) was mixed with the respective mAb solution (100 μL) and stirred at 500 rpm for 30 min. The mAb solution concentration was 40 μg mL^{-1} in the case of 8-OHdG, while caffeine and acetaminophen mAbs varied according to experiments as described in the text. Next, 100 μL of 10% (w/v) BSA solution and 50 μL of 1% (w/v) PEG 20 000 solution were added, followed by an additional 10 min of stirring. Then, 450 μL of 20 mM Tris–HCl buffer (pH = 8.2) containing 0.05% (w/v) PEG 20,000, 150 mM sodium chloride, 1% (w/v) BSA, and 0.1% (w/v) sodium azide was added, followed by centrifuging at 4 °C and 6500 rcf. Finally, the precipitate was resuspended in 15 mM Tris–HCl buffer (pH = 8.2) containing 2.5% (w/v) sucrose, 0.25% (w/v) BSA, 0.04% (w/v) PEG 20,000, 0.025% (w/v) sodium azide, and 110 mM sodium chloride, and adjusted to OD = 1.5 to be used as labeled mAb solutions for deposition onto conjugate pads.

Modification of NC membranes by inkjet printing

The standard cartridges (BC-345 Black and BC-346 Color) originally supplied with the printer were cut open. The sponge and
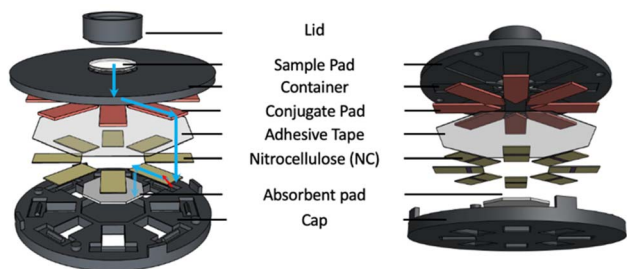

Fig. 1 Design of device type P with 8 LFIA lanes for plain non-backed nitrocellulose membranes; blue arrows represent the sample liquid flow path on the example of a single LFIA lane.

film were removed, followed by washing with ultra-pure water. The BC-345 cartridge was blocked with a 0.01% (w/v) BSA solution to prevent the nonspecific adsorption of proteins onto the inner wall of the plastic cartridge.

Target antigen-BSA conjugate solutions were diluted to 0.1 mg mL^{-1} by pure water and loaded into the BC-345 cartridge. These solutions were deposited onto NC membranes as a pattern designed in the Adobe Illustrator CC software. As mentioned in our previous report, the amount of deposited solution was controlled by the number of printing cycles.[45] A hairdryer blew cold air for 2 min between repeated printing runs. After the deposition, the NC membranes were dried at 37 °C for 2 h and stored in a desiccator (<25% humidity) until use.

Fabrication of 3D devices

Cellulose fiber used for absorbent pads was cut into a regular hexagon shape. Glass fiber used for sample, conjugate, and transfer pads was cut into circle, pentagon, and square shapes, respectively. The scale details for each type of pads are shown in Fig. S2.† The sample pad was treated with 50 μL of 0.2 M Tris–HCl buffer (pH = 8.5) containing 5% (w/v) PVP K25, and the conjugate pad was prepared by applying 35 μL of Au-mAb conjugate solution. Then, both sample pads and conjugate pads were dried at 37 °C for 2 hours. These prepared pads were mounted on the fixed positions of the 3D-printed container and cap. The double-sided adhesive film was used to seal conjugate pad channels and attach NC membranes to the conjugate pads. The completed devices were stored in a desiccator at room temperature (<20% humidity). The detailed design and dimensions of the devices are shown in Fig. S3 and S4.†

Characterization of multiplex analyte detecting devices

The essential characteristics of both device types, P and B, were evaluated using the combination of Au-anti-8-OHdG applied onto conjugate pads and 8-OHdG-BSA deposited on NC membranes. Ultrapure water was used for the preparation of 8-OHdG standard solutions. In addition, for semiquantitative target detection, the sample volume for device type P was optimized. The concentrations of labeled mAbs were optimized following the steps reported in previous work,[47] with 70 μg mL^{-1} of 8-OHdG mAb, 160 μg mL^{-1} of caffeine mAb, and acetaminophen mAb finally used. Different amounts of 8-OHdG, caffeine, and acetaminophen were dissolved in ultrapure water for further investigations to obtain a concentration-dependent signal. 20 minutes after applying the sample to the 3D device, images of the surface of NC membranes were captured with the scanner after removing the device cap. The colorimetric intensity of test lines was extracted as a "Δgray value" by the ImageJ software, as shown in Fig. S5.†

Characterization of text-displaying semiquantitative detection device

Device type P adapted for non-backed NC membranes was used. 140, 80, 60 μg mL^{-1} of caffeine mAb and 140, 120, 80, 60 μg mL^{-1} of acetaminophen mAb were used for labeling with AuNPs

for semiquantitative detection in combination with different numbers of printing cycles (5, 10, 15, 20 times) of caffeine- or acetaminophen-BSA conjugate. Artificial urine samples were prepared following a description by Brooks and Keevil (Table S1†).[48] Assays were conducted by adding 350 μL of artificial urine samples containing different concentrations of caffeine and acetaminophen, followed by selecting the lowest level of text symbol recognizable by the naked eye among all the lanes to represent the approximate range of the analyte concentration.

Results and discussion

Multiple configurations of nitrocellulose membranes are commercially available. Since plain nitrocellulose membranes are brittle and fragile, the most widely used configuration typically applied in commercial LFIA devices is produced on plastic backing support for stabilization. This work developed two types of devices, device P (accommodating plain NC membranes) and device B (accommodating plastic-backed NC membranes), to demonstrate maximum flexibility in design and application.

Plastic-backed NC membranes can be more easily manufactured, transported, and handled due to their enhanced robustness. However, this NC membrane is limited to two-dimensional flow since liquids cannot pass vertically through the substrate. For this reason, sample liquid application and signal detection are restricted to one side of the membrane, reducing device design flexibility in the context of multiplexed analyte detection. To overcome this limitation, a so-called "transfer pad" (TP) was introduced in the device of design B to build a three-dimensional flow channel. However, the TP increases the device complexity and requires a larger sample liquid volume for assay operation. The device of type P enables working with plain NC membranes, directly providing three-dimensional flow options.

Design and working principle for 3D-device type B

This eight-lane LFIA device was designed to accommodate plastic-backed nitrocellulose membranes. A circular concave area on the top face of the container was used to hold a single central sample pad, while eight concave channels on the back side were designed to hold individual conjugate pads. A double-sided adhesive tape was cut to a hexagon shape to attach the NC membranes and transfer pads (TP) to the back side of the conjugate pad. The cap was designed to be combined with the container at a fixed position to keep all pads in place. Eight rectangular windows corresponding to the eight LFIA lanes were arranged on the container to observe the detection signals from the bottom of the device. A small concave area in the center of the cap accommodates a single absorbent pad common to all lanes. A schematic cross-section of layer arrangement and sample liquid flow in a 3D device of type B is shown in Fig. 2. Details on the design of the cap sections with support protrusions serving the purpose of pressing the TPs onto the conjugate pads to guarantee reproducible liquid transfer are shown in Fig. S4.† After sample application into the
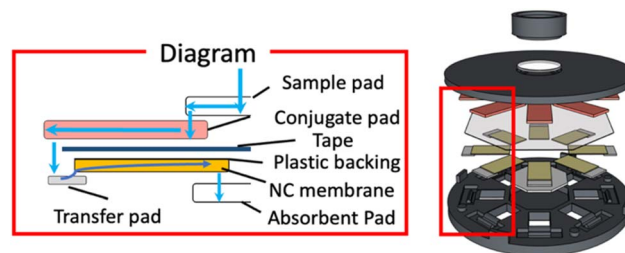

Fig. 2 Schematic diagram showing sample liquid flow path through a single assay lane of LFIA device type B.

lid, the liquid is absorbed by the sample pad in a short moment and equally distributed to the 8 conjugate pads *via* capillary forces. The sample solution redissolves the pre-deposited labeled antibodies, wicks horizontally to the outer edge, and transfers to the NC membrane through the TP (Fig. 2). The TP is necessary due to liquid impermeable plastic-backed NC membranes. The antigen-BSA conjugate is pre-deposited on the NC membranes as test lines. When the sample solution migrates to the position with deposited antigen-BSA conjugates, the labeled antibodies competitively bind either to the target antigens present in the sample or the inkjet-deposited antigen-BSA conjugates on the NC membrane. Finally, the results are displayed in the eight observation windows simultaneously. The central absorbent pad absorbs the remaining sample solution. The design of this device allows users to realize eight analytical tests within a short time with a single sample application.

Basic characterization of 3D-device type B

8-OHdG was used as a low molecular weight model analyte in a competitive immunoassay format to characterize device type B performance. Pure water was used to evaluate the equivalence of the eight LFIA lanes. The average Δgray value and its standard deviation were 38.15 ± 1.53. Therefore, similar signal intensities were confirmed in each lane of the device (Fig. 3), indicating that the centrally applied sample liquid is equally distributed into the conjugate pads and the nitrocellulose membrane strips.

In addition, a series of 8-OHdG samples at seven concentration levels was tested using seven independently fabricated devices (Fig. 4a). As expected from the known response behavior
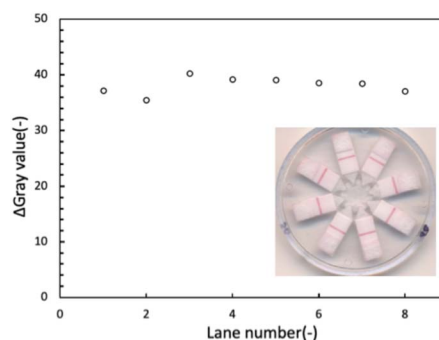

Fig. 3 Signal intensities recorded for each individual LFIA lane in a single device of type B after application of a blank sample.
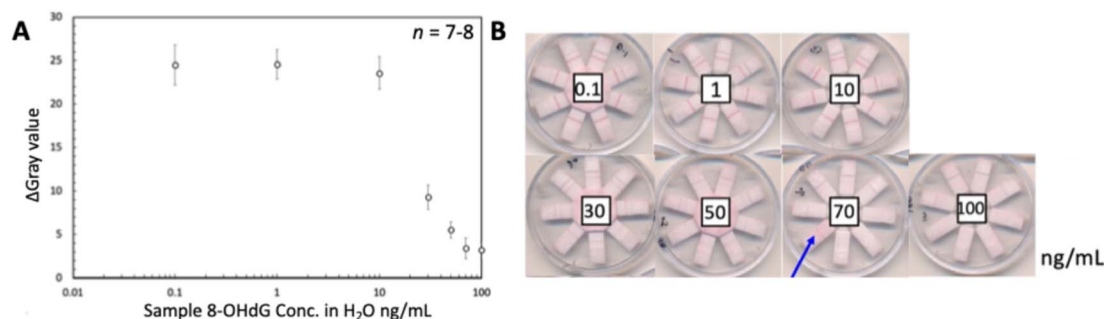
Fig. 4   (A) 8-OHdG concentration-dependent response of assays performed with device type B (8-OHdG = 0.1, 1, 10, 30, 50, 70, 100 ng mL^{-1}), and (B) color scans of corresponding devices; error bars represent one standard deviation from the mean (n = 7 or 8); blue arrow in (B) marks an LFIA lane with irregular flow behavior.

of the competitive LFIA format, the color intensities of all test lines weakened at concentrations above 10 ng mL^{-1}, until completely disappearing at high analyte concentrations. The observed concentration response range was similar to the one observed in our previous work.[45] The results shown in Fig. 4b revealed that one out of the total of 56 LFIA lanes (7 devices × 8 lanes) involved in this experiment exhibited a strong background signal (8-OHdG concentration of 70 ng mL^{-1}). This irregularity was attributed to insufficient contact and overlap between the NC membrane and the absorbent pad, resulting in incomplete liquid transport and hence, insufficient washing out of unbound signaling antibody. It should be noted that all devices have been individually manually assembled. The reproducible results obtained on 55 of the totals of 56 assay lanes indicate the satisfactory performance of the LFIA devices.

Detection of multiplex samples with 3D-device type P

Plain NC without plastic backing was applied for 3D-device type P, and the schematic liquid flow path through an LFIA lane is shown in Fig. 5. Due to the absence of the plastic backing, the sample flow is directly transferred from the conjugate pad to the back side of the NC without the requirement for a TP. To accommodate the different types of NC, the device cap was modified, as shown in Fig. S3c.† Four pieces of each conjugate pad loaded with pre-deposited Au-anti-caffeine or Au-anti-acetaminophen were placed into the eight channels. To force the sample flow through the entire conjugate pad and to gain sufficient time for the immunocomplex formation, the double-sided adhesive tape here served as a flow control film to prevent the sample liquid from directly penetrating through the conjugate pad into the back side of the NC membrane. The caffeine/acetaminophen-BSA conjugates were printed on the NC membrane as test lines to capture free AuNP-labelled anti-caffeine or anti-acetaminophen antibodies. Finally, the results are interpreted through the eight windows.

First, one disadvantage of working with multiplexed LFIA devices with a multi-channel design is the generally larger sample volume required. Different volumes (300, 350, 400 μL) of blank samples were applied to devices with eight caffeine-targeting LFIA lanes to identify the minimally necessary amount of sample for the device designed in this work. The
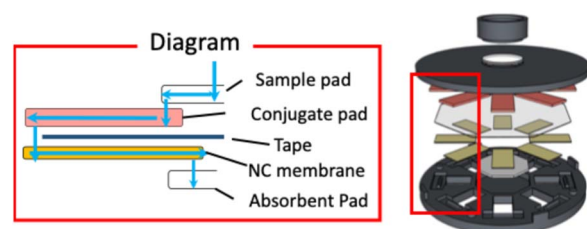

Fig. 5   Schematic diagram showing sample liquid flow path through a single assay lane of LFIA device type P.

Δgray values averaged over all eight lanes in a single device are shown in (Fig. 6). Although 300 μL was sufficient to operate the device, 350 μL was selected as the optimal minimally required sample liquid volume because it showed a higher signal intensity.

To demonstrate the working of this device and, importantly, to verify that there is no crosstalk between the LFIA lanes targeting different analytes, samples containing only a single analyte or a mixture thereof were analyzed. The results are shown in Fig. 7. Data analysis revealed no significant
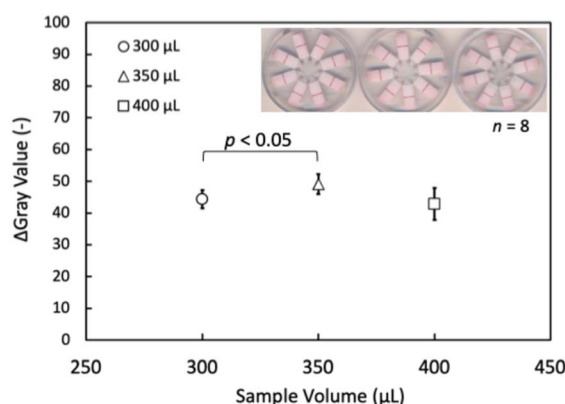

Fig. 6   Signal intensities observed for blank samples (caffeine LFIA) after application of various sample volumes to LFIA device type P; the inset shows the actually observed test lines on devices after application of 300, 350 and 400 μL of sample liquid; error bars represent one standard deviation from the mean (n = 8; signal acquired from 8 lanes of a single device).
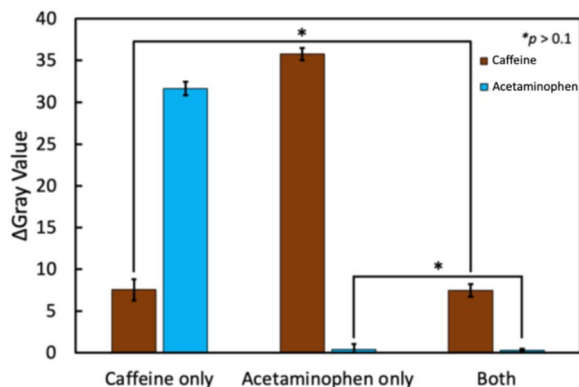
Fig. 7 Signal intensities observed for samples containing a single target (200 ng mL^{-1} of caffeine or acetaminophen) or a mixture (caffeine = 200 ng mL^{-1} and acetaminophen = 200 ng mL^{-1}) on LFIA device type P; error bars represent one standard deviation from the mean ($n = 4$; signal acquired from 4 lanes of a single device).
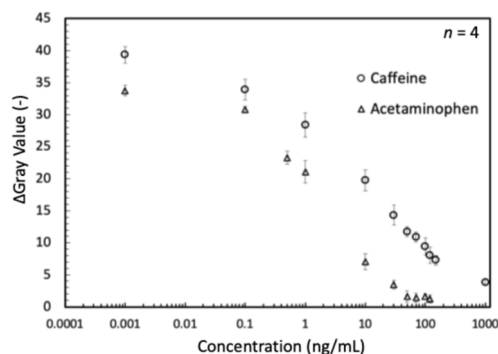

Fig. 8 Analyte concentration-dependent response of assays performed with device type P for mixed samples containing both caffeine and acetaminophen (caffeine = 0, 0.1, 1, 10, 30, 50, 70, 100, 120, 150, 1000 ng mL^{-1}, acetaminophen = 0, 0.1, 0.5, 1, 10, 30, 50, 70, 100, 120, 150 ng mL^{-1}); error bars represent one standard deviation from the mean ($n = 4$; signal acquired from 4 lanes of a single device).

differences between the positive signals obtained with samples containing a single analyte or mixed samples. Finally, concentration-dependent response curves were recorded with

11 mixed samples, including caffeine and acetaminophen (Fig. 8).

Principle of semi-quantitative signal detection

In competitive lateral flow immunoassays, quantitative information gained in test line color intensities strongly depends on the ratio of reagents deposited in the conjugate pad (labeled detection antibodies) and the NC membrane (capture reagents). Adjusting these amounts during LFIA device optimization enables tuning concentration threshold values that lead to weakening and finally disappearance of test lines as a function of target analyte concentration. In a conventional approach, results are judged by counting the number of disappeared test lines made with different concentrations of capture reagents deposited.[32] In this work, we aimed at using the modulation of the ratio of labeled detection antibodies pre-deposited on the conjugate pads to the antigen-BSA conjugates inkjet deposited as capture reagents in line or text form on the NC membranes to enable semi-quantitative judgment of approximate target analyte concentration ranges by the naked-eye reading of the visible results. Based on the equilibrium equation of antibody–antigen interactions (eqn (S1)†), the level of immunocomplex formed can be controlled by changing the initial concentrations of antibody or antigen. In other words, to achieve different test line or text symbol intensities at a constant concentration of target antigen, it is adequate to change the density of AuNP-labeled antibodies on the conjugate pad or the amount of BSA-conjugates inkjet-printed on the NC membrane. Based on these considerations, a single eight-lane LFIA device of type P was prepared with eight different AuNP-mAb to BSA-conjugate ratio conditions for both caffeine and acetaminophen detection. The level of BSA-conjugate on the NC membrane was readily modified by varying the number of repeated printing cycles, as already done in our previously reported work.[45] The target antigen concentration-dependent response curves for caffeine and acetaminophen are shown in Fig. 9. Four response curves with different AuNP-mAb to BSA-conjugate ratios have been prepared for both analytes. By variations in this ratio, tuning the amount of immunocomplex formed at the test line is possible. Therefore, by tuning the threshold value for complete test line disappearance to different
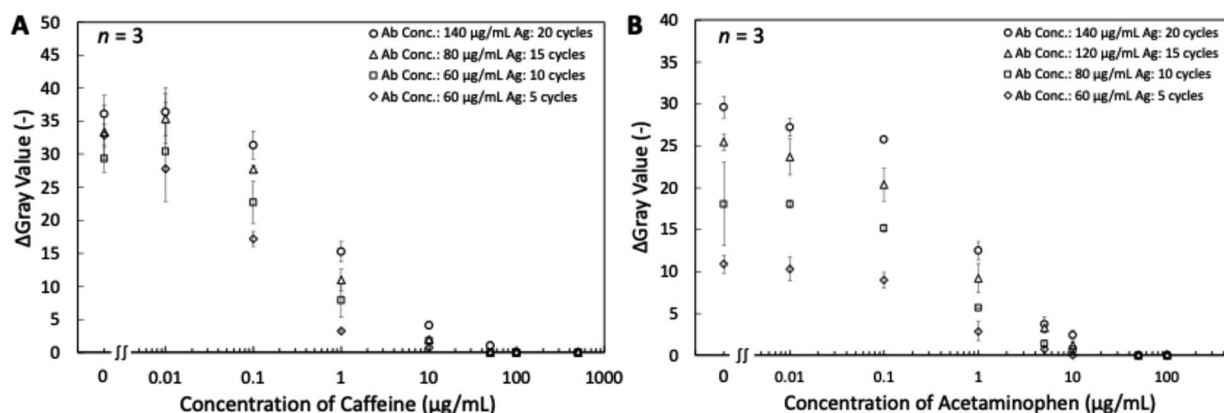

Fig. 9 Different dynamic response ranges for target analytes in artificial urine matrix: caffeine (A), acetaminophen (B) achieved by adjusting the amount of labeled antibody deposited on conjugate pads and inkjet printing cycles of BSA-conjugates on the NC membrane; error bars represent one standard deviation from the mean ($n = 3$).
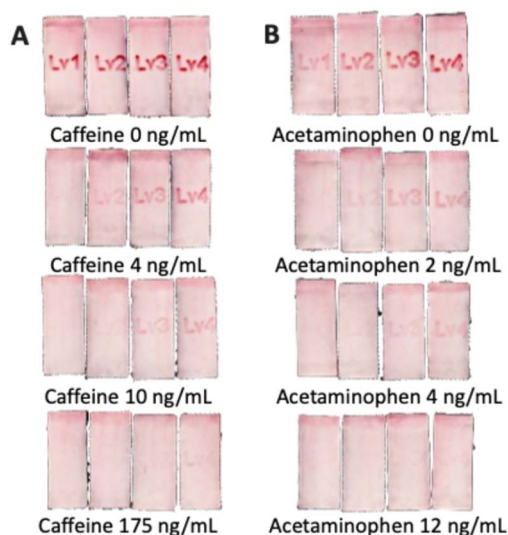
Fig. 10 Text-displaying results for the semi-quantitative detection of (A) caffeine = 0, 4, 10, 175 ng mL^{-1}, (B) acetaminophen = 0, 2, 4, 12 ng mL^{-1} in artificial urine samples. The figure shows a zoom-in to each LFIA lane on a single device; brightness, contrast and saturation have been modified to improve visibility; the unmodified originals of overall devices are shown in Fig. S6.†

target concentrations, users can identify the approximate analyte concentration range for an unknown sample with the naked eye.

Text-displaying semi-quantitative signal detection

Based on the results discussed in the previous section, capture reagents (BSA-conjugates) have been inkjet printed on the NC membranes in text form with the optimized number of printing cycles for controlling the visibility or disappearance of text. For each analyte, the lowest level of readable text (levels 1–4) represents the approximate range of the target analyte concentration. Four sets of artificial urine samples with caffeine and acetaminophen mixtures have been applied to verify different concentration levels. The actual applied concentrations and the visual text appearance in the single LFIA lanes are shown in Fig. 10, while the results have been summarized in Table 1. Pictures of the entire devices are shown in Fig. S6.† The green blocks indicate the text is visible at the specific analyte concentrations, while the red blocks indicate that the text is invisible. With increasing analyte concentrations, the text disappears, starting with the one pointing to the lowest concentration. Therefore, the developed eight-lane LFIA device enabled the simultaneous semi-quantitative naked-eye detection of two

analytical targets at 4 concentration levels in the competitive immunoassay format.

Conclusions

In this work, two 3D-printed devices integrating eight LFIA lanes have been designed to realize a competitive immunoassay format, demonstrating the potential for simultaneous multiplex target detection or naked eye semi-quantitative analyte detection through single application of a comparably low sample volume. Focus was set on a compact but flexible design to accommodate multiple flow paths with a central sample inlet. The equivalence of the eight LFIA lanes allows multiplexed and semi-quantitative analyte detection free of crosstalk, while maintaining all advantages of the well-known conventional LFIA strips. The device design enables the use of both plastic backed and bare nitrocellulose membranes, coping with the recently limited market availability of specific NC membrane materials. Naked eye semi-quantitative signal detection was achieved by adjusting the amount of AuNP-conjugated detection antibodies in the conjugate pads and inkjet printed capture reagents on the NC membranes, resulting in gradually disappearing text symbols with increasing analyte concentrations. The use of inkjet printed text symbols provides the possibility of tuning text disappearance concentration thresholds and enables intuitive signal readout. The performance of devices has been evaluated for several model analytes, demonstrating the detection of 8-OHdG, caffeine and acetaminophen. The developed concept thus paves the way for further applications to either multiplexed or semi-quantitative target antigen analysis.

Data availability

Data created and analyzed in this study are included in the article and the ESI file.† Raw data supporting the findings of this study are available from the corresponding author upon reasonable request.

Author contributions

Guodong Tong: conceptualization, methodology, investigation, data curation, formal analysis, writing – original draft. Kazushi Misawa: conceptualization, methodology, investigation, supervision. Purim Jarujamrus: validation, writing – review & editing, supervision. Yuki Hiruta: validation, writing – review & editing, supervision, funding acquisition. Daniel Citterio: conceptualization, methodology, validation, writing – review & editing, supervision, project administration, funding acquisition.

Conflicts of interest

There are no conflicts to declare.

Acknowledgements

Table 1 Naked eye judgement of visible results related to each analyte

Targets	Caffeine				Acetaminophen			
Conc. (ng/mL)	Lv. 1	Lv. 2	Lv. 3	Lv. 4	Lv. 1	Lv. 2	Lv. 3	Lv. 4
C.=0 A.=0	🟩	🟩	🟩	🟩	🟩	🟩	🟩	🟩
C.=4 A.=4	🟥	🟩	🟩	🟩	🟥	🟩	🟩	🟩
C.=10 A.=8	🟥	🟥	🟩	🟩	🟥	🟥	🟩	🟩
C.=175 A.=12	🟥	🟥	🟥	🟩	🟥	🟥	🟥	🟩

Visible: 🟩 Invisible: 🟥

References

1 J. R. Choi, K. W. Yong, R. Tang, Y. Gong, T. Wen, H. Yang, A. Li, Y. C. Chia, B. Pingguan-Murphy and F. Xu, *Adv. Healthcare Mater.*, 2017, **6**, 1600920.

2 X. Wang, K. Li, D. Shi, N. Xiong, X. Jin, J. Yi and D. Bi, *J. Agric. Food Chem.*, 2007, **55**, 2072–2078.

3 Y. Zhao, H. Wang, P. Zhang, C. Sun, X. Wang, X. Wang, R. Yang, C. Wang and L. Zhou, *Sci. Rep.*, 2016, **6**, 21342.

4 J. B. Old, B. A. Schweers, P. W. Boonlayangoor and K. A. Reich, *J. Forensic Sci.*, 2009, **54**, 866–873.

5 R. Wang, W. Zhang, P. Wang and X. Su, *Microchim. Acta*, 2018, **185**, 191.

6 Z. Xie, D. Kong, L. Liu, S. Song and H. Kuang, *Food Agric. Immunol.*, 2017, **28**, 439–451.

7 M. Zhang, L. Yan, Q. Huang, T. Bu, S. Yu, X. Zhao, J. Wang and D. Zhang, *Food Control*, 2018, **84**, 215–220.

8 J.-H. Lin, C.-M. Lo, S.-H. Chuang, C.-H. Chiang, S.-D. Wang, T.-Y. Lin, J.-W. Liao and D.-Z. Hung, *PLoS Neglected Trop. Dis.*, 2020, **14**, e0008701.

9 A. V. Bartosh, D. V. Sotnikov, O. D. Hendrickson, A. V. Zherdev and B. B. Dzantiev, *Biosensors*, 2020, **10**, 17.

10 Q. Mei, B. Ma, J. Li, X. Deng, J. Shuai, Y. Zhou and M. Zhang, *Food Chem.*, 2024, **439**, 138171.

11 G. M. S. Ross, G. I. Salentijn and M. W. F. Nielen, *Biosensors*, 2019, **9**, 143.

12 L. Lin, X. Xu, S. Song, L. Xu, X. Wu, L. Liu, H. Kuang and C. Xu, *Food Chem.*, 2022, **377**, 131964.

13 D. Zhao, J. Liu, J. Du, K. Liu and Y. Bai, *Food Measure*, 2023, **17**, 6577–6587.

14 Z. Li, Y. Yi, X. Luo, N. Xiong, Y. Liu, S. Li, R. Sun, Y. Wang, B. Hu, W. Chen, Y. Zhang, J. Wang, B. Huang, Y. Lin, J. Yang, W. Cai, X. Wang, J. Cheng, Z. Chen, K. Sun, W. Pan, Z. Zhan, L. Chen and F. Ye, *J. Med. Virol.*, 2020, **92**, 1518–1524.

15 H. Jiang, H. Su, K. Wu, Z. Dong, X. Li, L. Nie, Y. Leng and Y. Xiong, *Sens. Actuators, B*, 2023, **374**, 132793.

16 S. Hou, J. Ma, Y. Cheng, H. Wang, J. Sun and Y. Yan, *Food Control*, 2020, **117**, 107107.

17 G. Xue, M. Wu, T. Liu, X. Fang, J. Yin, W. Lai and J. Peng, *J. Dairy Sci.*, 2023, **106**, 3856–3867.

18 Q. Wang, Y. Liu, M. Wang, Y. Chen and W. Jiang, *Anal. Bioanal. Chem.*, 2018, **410**, 223–233.

19 M. Han, L. Gong, J. Wang, X. Zhang, Y. Jin, R. Zhao, C. Yang, L. He, X. Feng and Y. Chen, *Sens. Actuators, B*, 2019, **292**, 94–104.

20 J. Peng, Y. Wang, L. Liu, H. Kuang, A. Li and C. Xu, *RSC Adv.*, 2016, **6**, 7798–7805.

21 C. Xing, L. Liu, S. Song, M. Feng, H. Kuang and C. Xu, *Biosens. Bioelectron.*, 2015, **66**, 445–453.

22 N. A. Taranova, N. A. Byzova, V. V. Zaiko, T. A. Starovoitova, Y. Y. Vengerov, A. V. Zherdev and B. B. Dzantiev, *Microchim. Acta*, 2013, **180**, 1165–1172.

23 J. Li and J. Macdonald, *Lab Chip*, 2016, **16**, 242–245.

24 L. Wang, J. Cai, Y. Wang, Q. Fang, S. Wang, Q. Cheng, D. Du, Y. Lin and F. Liu, *Microchim. Acta*, 2014, **181**, 1565–1572.

25 R. H. Sayed, R. T. Soliman and S. A. Elsaady, *J. Adv. Vet. Anim. Res.*, 2023, **10**, 292–300.

26 Y. Zhao, H. Wang, P. Zhang, C. Sun, X. Wang, X. Wang, R. Yang, C. Wang and L. Zhou, *Sci. Rep.*, 2016, **6**, 21342.

27 A. N. Berlina, N. A. Taranova, A. V. Zherdev, Y. Y. Vengerov and B. B. Dzantiev, *Anal. Bioanal. Chem.*, 2013, **405**, 4997–5000.

28 H. Lei, K. Wang, X. Ji and D. Cui, *Sensors*, 2016, **16**, 2130.

29 X. Zhu, M. Sarwar, J.-J. Zhu, C. Zhang, A. Kaushik and C.-Z. Li, *Biosens. Bioelectron.*, 2019, **126**, 690–696.

30 S. Zhang, X. Jiang, S. Lu, G. Yang, S. Wu, L. Chen and H. Pan, *Sensors*, 2023, **23**, 6401.

31 R. Xiao, L. Lu, Z. Rong, C. Wang, Y. Peng, F. Wang, J. Wang, M. Sun, J. Dong, D. Wang, L. Wang, N. Sun and S. Wang, *Biosens. Bioelectron.*, 2020, **168**, 112524.

32 E. A. Zvereva, N. A. Byzova, P. G. Sveshnikov, A. V. Zherdev and B. B. Dzantiev, *Anal. Methods*, 2015, 7, 6378–6384.

33 A. H. Iles, P. J. W. He, I. N. Katis, P. P. Galanis, A. J. U. K. John, P. Elkington, R. W. Eason and C. L. Sones, *Talanta*, 2022, **237**, 122944.

34 S. Zhang, Y. Sun, Y. Sun, H. Wang and Y. Shen, *Microchim. Acta*, 2020, **187**, 447.

35 J. M. Rosenbohm, C. M. Klapperich and M. Cabodi, *Anal. Chem.*, 2022, **94**, 3956–3962.

36 D. Li, M. Huang, Z. Shi, L. Huang, J. Jin, C. Jiang, W. Yu, Z. Guo and J. Wang, *Anal. Chem.*, 2022, **94**, 2996–3004.

37 M. Sharafeldin, K. Kadimisetty, K. S. Bhalerao, T. Chen and J. F. Rusling, *Sensors*, 2020, **20**, 4514.

38 S. S. Kanani, H.-Y. Tsai and W. R. Algar, *Anal. Chem.*, 2023, **95**, 13258–13265.

39 Y. Jiao, C. Du, L. Zong, X. Guo, Y. Han, X. Zhang, L. Li, C. Zhang, Q. Ju, J. Liu, H.-D. Yu and W. Huang, *Sens. Actuators, B*, 2020, **306**, 127239.

40 H. Ordutowski, C. Parra-Cabrera, C. Achille, R. Dochy, F. D. Dosso, J. Lammertyn, R. Ameloot and D. Spasic, *Appl. Mater. Today*, 2023, **32**, 101788.

41 M. Zangheri, L. Cevenini, L. Anfossi, C. Baggiani, P. Simoni, F. Di Nardo and A. Roda, *Biosens. Bioelectron.*, 2015, **64**, 63–68.

42 X. Ruan, Y. Wang, E. Y. Kwon, L. Wang, N. Cheng, X. Niu, S. Ding, B. J. Van Wie, Y. Lin and D. Du, *Biosens. Bioelectron.*, 2021, **184**, 113238.

43 J. Park and J.-K. Park, *Sens. Actuators, B*, 2017, **246**, 1049–1055.

44 F.-J. Cao, H.-H. Cheng, S.-X. Ma, F. Jiao and D.-M. Dong, *Sens. Bio-Sens. Res.*, 2022, **38**, 100533.

45 K. Misawa, T. Yamamoto, Y. Hiruta, H. Yamazaki and D. Citterio, *ACS Sens.*, 2020, **5**, 2076–2085.

46 M. Cui, R. Liu, Z. Deng, G. Ge, Y. Liu and L. Xie, *Nano Res.*, 2014, **7**, 345–352.

47 N. A. Byzova, I. V. Safenkova, E. S. Slutskaya, A. V. Zherdev and B. B. Dzantiev, *Bioconjugate Chem.*, 2017, **28**, 2737–2746.

48 T. Brooks and C. W. Keevil, *Lett. Appl. Microbiol.*, 1997, **24**, 203–206.